American Journal of Engineering Research (AJER) 2016
American Journal of Engineering Research (AJER)
e-ISSN: 2320-0847 p-ISSN : 2320-0936
Volume-5, Issue-3, pp-132-139
www.ajer.org
Research Paper Open Access

Investigation into Unsteady Blade Row Interaction Effects of a Two-Stage Counter-Rotating Lift-Fan by Harmonic Balance Method

Xiang Zhang[1], XiuQuan Huang[1], HengMing Zhang[1], YuChun Chen[1]
[1](School of power and energy, Northwestern Polytechnical University, China)

ABSTRACT: *Applying the harmonic balance method, an effective computational method in simulating time-periodic unsteady flows, this article studied the unsteady blade row interaction effects of a two-stage counter-rotating lift-fan. The unsteady flow in the 1st blade row was represented by one harmonic wave, while the unsteady flow of the 2nd blade row was modeled using three harmonic waves. The results show that: (1) the isentropic efficiency and lift force are proportional to the rotate speed, with the maximum of 88.35% and 130.04N respectively at the design speed; (2) the harmonic balance method predicts a higher isentropic efficiency of the 2nd rotor below its mid-span than the steady study, while a contrary observation is obtained above the mid-span; (3) the harmonic balance method is efficient and reliable to simulate the time-periodic unsteady blade row interaction.*

Keywords - *Harmonic Balance, Unsteady Flow, Lift-Fan, Counter-Rotating, Blade Row Interaction*

I. INTRODUCTION

Lift fan as the direct lift device, has a broad prospect in military and civil applications. In recent years, it has been successfully used in the vertical take-off and landing (VTOL) aircraft. A typical example is the Mule series VTOL unmanned aerial vehicles (UAV) developed by Israel Urban Aero. The maximum take-off weight of Mule is 1,130kg with a cargo capacity of 226kg. Another example is the counter-rotating lift fan in F-35B designed by Lockheed Martin Corporation.

In this article, a two-stage counter-rotating lift fan, designed to power a small flying saucer, is studied. By canceling the stators, the counter-rotating fan is more compact, and the flow unsteadiness induced the blade row interaction is strong. Recently, more research effort has been spent to investigate the unsteady flow in counter-rotating fans.

Most of unsteady flow field simulations are based on time domain, which are high computational time costly and hinder engineering application. The unsteady effects of turbomachinery can be divided into conditioned unsteady and inherent unsteady. The conditioned unsteady effects means the unsteady phenomenon would happen at specified working condition, for example, rotating stall and surge, while the inherent unsteady effects arise from blade row interaction, which makes the flow change periodically. And the inherent unsteady effects are considered to be the dominant part in the turbomachinery unsteady flow. For these characteristics of the unsteady flow in turbomachinery, an effective method with the ability to capture the inherent unsteady effects is proposed, which represents these changing flow variables by Fourier series approximately. By that, the unsteady calculation can be translated from time domain to frequency domain and reaches the objective of time savings. The frequency domain methods include the time-linearized linear/nonlinear harmonic method, the Harmonic Balance Method, the Nonlinear Frequency Domain method and the Nonlinear Harmonic Phase Solution method. The time-linearized equations were obtained by subtracting the time-averaged equations from the original unsteady flow equations and neglecting the nonlinear terms (Adamczyk, 1985[1]). And Hall and Lorence[2] expressed this unsteady time-linearized equations as one harmonic. With the harmonic formulation, the time domain unsteady time-linearized equations could be converted into steady like equations about the harmonic amplitude in the frequency domain. The use of the Fourier transformation technique was further exploited by Hall[3] and McMullen[4]. Hall proposed the Harmonic Balance Method, while McMullen proposed the Nonlinear Frequency Domain method. And the latest Nonlinear Harmonic Phase Solution method is coined by He[5].

This article adopts the Harmonic Balance method for unsteady flow field simulation. This method expresses an unsteady flow solution as a whole in Fourier series, giving rise to work out the time derivative in the unsteady flow equations using the flow solution at equally spaced phases in a period of unsteadiness. Fourier transformation is utilized to get the time derivatives of the conservative flow variables in terms of the flow solution variables at those discrete phases.

II. PHYSICAL MODEL AND SOLUTION METHOD

Integrating the unsteady Reynolds-averaged Navier-Stokes (U-RANS) equations over a control volume, we could obtain the following semi-discrete finite-volume form equations:

$$V\frac{\partial \boldsymbol{W}}{\partial t}+R(\boldsymbol{W})=0 \tag{1}$$

where $\boldsymbol{W}$ is the conservative flow variables, including the fluid density, momentum, total energy and turbulent variables depending on the model; V represents the volume of the grid cell and R is the residual resulting from the discretization of the fluxes and the source terms (comprising the turbulent equations).

Assuming the flow variables are composed of non-harmonically related frequencies, these variables could be expressed approximately as follow :

$$\boldsymbol{W}(t)\approx\sum_{k=-N}^{N}\hat{\boldsymbol{W}}_k e^{i\omega_k t} \tag{2}$$

$$\boldsymbol{R}(t)\approx\sum_{k=-N}^{N}\hat{\boldsymbol{R}}_k e^{i\omega_k t} \tag{3}$$

where $\hat{\boldsymbol{W}}_k$ and $\hat{\boldsymbol{R}}_k$ are the coefficients of the Fourier series for the frequency $\Gamma_k=\omega_k/2\pi$. Plugging the Eq.(2) and the Eq. (3) into Eq.(1) yields

$$\sum_{k=-N}^{N}(i\omega_k V\hat{W}_k+\hat{R}_k)e^{i\omega_k t}=0 \tag{4}$$

The formula(4) could be changed into 2*N*+1 frequency domain equations by harmonic balance. However it is very different to solve it. By inverse discrete Fourier transformation, we could sample these equations in time onto a set of 2*N*+1 time levels. The following matrix formulation is obtained:

$$F^{-1}\cdot(iVP\hat{W}^{*}+\hat{R}^{*})=0 \tag{5}$$

F^{-1} is an inverse discrete Fourier transform matrix (IDFT) :

$$F^{-1}=\begin{bmatrix} e^{i\omega_{-N}t_0} & \cdots & e^{i\omega_0 t_0} & \cdots & e^{i\omega_N t_0} \\ \vdots & & \vdots & & \vdots \\ e^{i\omega_{-N}t_k} & \cdots & e^{i\omega_0 t_k} & \cdots & e^{i\omega_N t_k} \\ \vdots & & \vdots & & \vdots \\ e^{i\omega_{-N}t_{2N}} & \cdots & e^{i\omega_0 t_{2N}} & \cdots & e^{i\omega_N t_{2N}} \end{bmatrix}$$

Where,

$$\omega_0=0,\ t_0=0,\ \omega_{-N}=-\omega_N$$

$$P=diag(-\omega_N,\ldots,\omega_0\ldots,\omega_N)$$

$$\hat{W}^{*}=[\hat{W}_{-N},\ldots,\hat{W}_0,\ldots,\hat{W}_N]^{T},\quad \hat{R}^{*}=[\hat{R}_{-N},\ldots,\hat{R}_0,\ldots,\hat{R}_N]^{T}$$

So the Fourier coefficients can be computed by

$$\hat{W}^{*}=FW^{*} \tag{6}$$

$$\hat{R}^{*}=FR^{*} \tag{7}$$

$$W^* = [W(t_0), \ldots, W(t_i), \ldots, W(t_{2N})]^T; \quad R^* = [R(t_0), \ldots, R(t_i), \ldots, R(t_{2N})]^T$$

applying these relationships, the governing equations could be given by:

$$iVF^{-1}PFW^* + R^* = 0$$

By introducing the pseudo-time derivative term to the above equations, we can solve these equations by a time marching method.

As for spatial discretization, the central difference method with a second order and fourth order blended artificial viscosity is adopted. About temporal discretization, this article applies the four-stage Runge-Kutta method with second-order accuracy. In order to reduce time cost, local time stepping, implicit residual smoothing and multi-grid techniques are employed to accelerate convergence. The one-equation S-A model is chosen as turbulence model.

There are four types of boundary conditions. At the subsonic inlet boundary, the total pressure, total temperature and flow angles are specified, while the static pressure is prescribed at the outlet boundary. The non-reflecting boundary described by Giles[6] has been applied at both inlet and outlet boundary. The periodical boundary condition in a single blade passage computation for unsteady is different from the steady one. It is necessary to use the phase-lag condition[7] to take the space-time periodicity into account. Applying this condition in equation(2), we can obtain that:

$$\hat{W}_k(\theta + \Delta\theta, t) = \hat{W}_k(\theta, t) \cdot \exp(i\beta_k)$$

Where, β_k is the inner blade phase angle. Combining the Fourier transform equation(6), the periodical boundary condition in this article could be given by:

$$W^*(\theta + \Delta\theta) = F^{-1}MFW^*(\theta)$$

Where, $M = diag(-\beta_N, \ldots, \beta_0, \ldots, \beta_N)$

III. CASE DESCRIPTION

An original-designed two-stage counter-rotating lift fan is studied in the present work, which is the central part of the propulsion system. The 3D solid modeling drawing of this fan is showed in Fig.1.

Figure 1. Two-Stage Counter-Rotating Lift Fan

This fan is small with a constant shroud-contour radii of 75mm. The rate of mass flow and total pressure ratio at design point is 1.8 kg/s and 1.08 respectively. Before simulating this fan with harmonic balance method, we should give the frequencies of unsteady disturbance. According to Tyler and Sofrin[8], in multi-stage environment, the kth frequencies of jth row could be given by:

$$\omega_k^j = \sum_{i=1}^{NR} n_{k,i} B_i (BPF_i - BPF_j) \tag{8}$$

Where BPF means blade passing frequency, NR is blade count. The $n_{k,i}$ represents k sets of user-defined integers that drive the frequency combinations.

Table 1 Parameters about the unsteady frequency

	Design Rotation Speed(RPM)	Blade Count	BPF(Hz)
Row 1	-19100	7	318.3
Row 2	13200	8	220.0

According to the parameters in Table 1, specified $n_{1,2}$ =1 for blade row 1, then we can get that ω_1^1 =4306.7Hz, specified $n_{1,1}$ =1, 2, 3 for blade row 2, then we can get that ω_1^2 = 3768.3Hz, 7536.7Hz, 11305.0Hz.

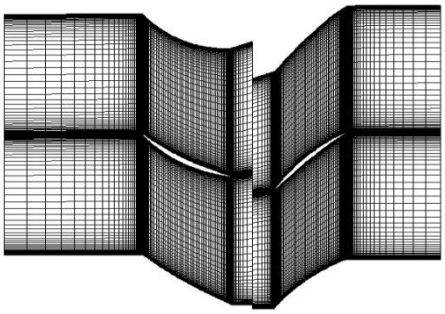

Figure 2. Computational Grid

Because of the adoption of phase-lag boundary condition, a single passage computational domain is used. In present work, single H block are applied on spatial discretization for each blade row. Both single H block have the same grid points in three direction, with 57×129×65 nodes in the circumferential, axial and radial direction respectively. The mesh is showed in Fig. 2.

IV. RESULTS AND DISCUSSION

Considering the atmosphere condition that the lift fan works at, total pressure (101325Pa) and total temperature (288.15K) is given at inlet and static pressure (101325Pa) is fixed at outlet. Then keeping the boundary conditions unchanged, several simulations using harmonic balance method have been finished at different rotation speed. The characteristic of lift force and isentropic efficiency varying with rotation speed is illustrated in Fig.3.

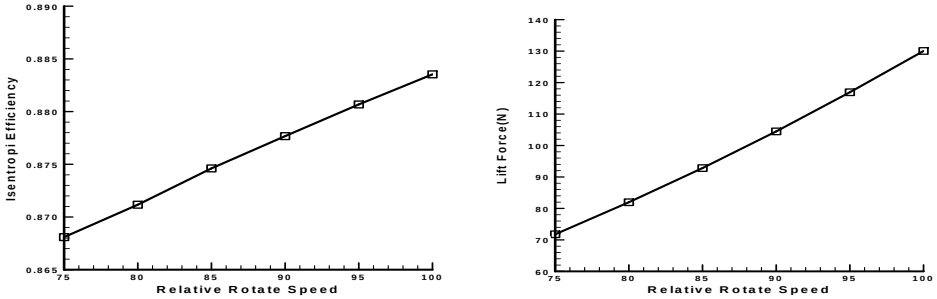

Figure 3. Lift Fan Characteristic: Lift Force and Isentropic Efficiency

The relative rotation speed is scaled by design rotation speed. Fig. 3 shows that the isentropic efficiency and lift force is almost linearly associated with the rotate speed. And the efficiency and lift force reach peak at design rotation speed, with 0.8835 and 130.04(N) respectively.

For further analysis, this article takes the working condition, i.e. design point, as the research object. By reconstructing the flow solution from harmonic balance in time, we can gain the time-varying flow variables. Fig. 4 shows the time-varying isentropic efficiency of row 1 and row 2.

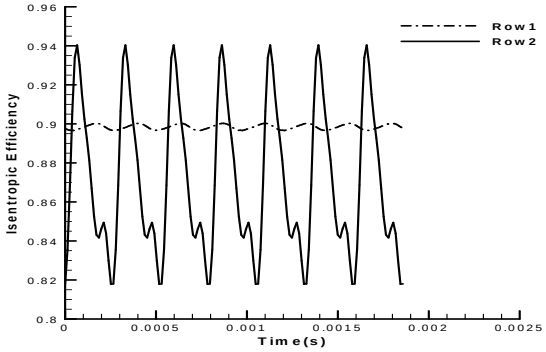

Figure 4. Variation of Isentropic Efficiency along Time at Design Point

From Fig. 4, it is clear that the isentropic efficiency in row 1 changed between 0.897 and 0.900, while it changed between 0.818 and 0.940 for row 2. So the changing amplitude for row 2(0.122) is almost as 40 times as that for row 1(0.003). This indicates that the flow unsteadiness in row 2 outweigh the flow unsteadiness in row 1.

The reason is that the dominant unsteady perturbation of row 1 is an acoustic disturbance (pressure wave), which is from row 2 and propagate both upstream and downstream for subsonic flow. And the unsteady perturbation of row 2 is composed of acoustic disturbance and entropy disturbance. The entropy disturbance is caused by the wake of row 1 and convects at a local flow velocity, running downstream. Entropy has a close relationship with the isentropic efficiency. As a result, the downstream of entropy disturbance of second row experiences a bigger variation of isentropic efficiency. The entropy could be compute as follow:

$$entropy = C_p \ln \frac{T}{T_{ref}} - R_g \ln \frac{P}{P_{ref}}$$

Where, T_{ref} is the reference temperature and P_{ref} is the reference pressure. In present work, T_{ref} equals inlet total temperature(288.16K) and P_{ref} equals inlet total pressure (101325Pa). Fig. 5 shows the process of wake entropy flow chopped by the second stage rotor.

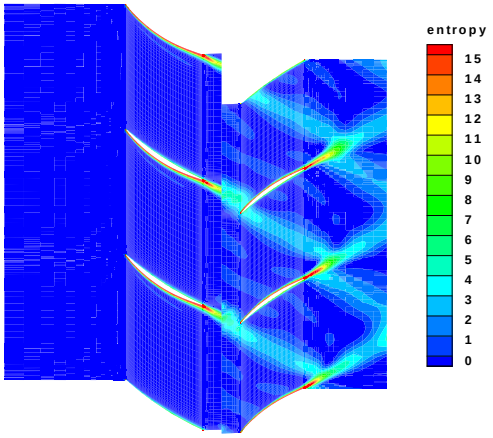

Figure 5. Instantaneous Entropy Contour of at 50% Span

In view of the small unsteady effects of row 1 and the difficulty of ensuring the performance of the second row of counter-rotating compressor/fan, it is more meaningful to study the unsteady effects of the second row. The follow part would focus on the unsteady flow field of the second row at design rotation speed.

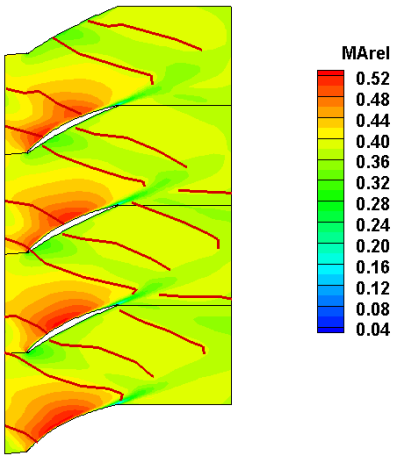

Figure 6. Instantaneous Relative Mach Number Contour at 20% Span of Row 2

Fig. 6 shows the instantaneous relative mach number contour of row 2, and the red solid lines represent the row1 wake shape. We can see that the originally arc-shaped relative-high mach regions are deformed by the rotor wakes. When the wakes pass through these arc regions, the area of these regions become smaller. It results from the negative jet described by Fig. 7.

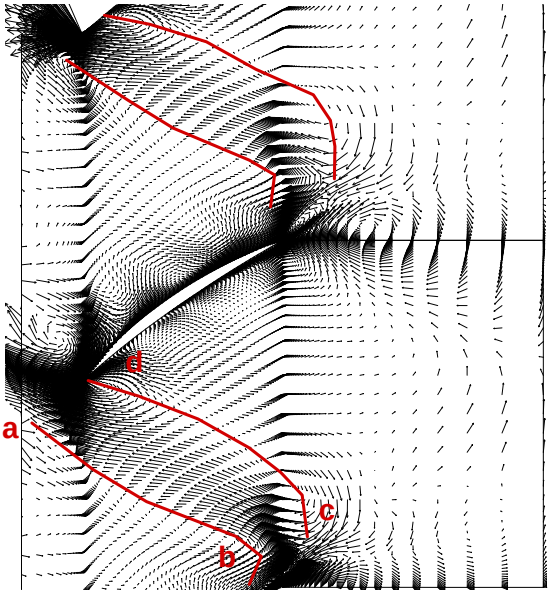

Figure 7. Instantaneous Velocity Vector Perturbation Field at 50% Span

The perturbation field is defined as the difference between an instantaneous solution and the time-averaged one. The wakes appear as a jet pointing upstream toward the trailing edge of the blade it originated from. So the direction of disturbance velocity is opposing the direction of mean flow velocity. As a result, it lessens the mach number and causes the deformation of high relative mach number region. According to the model of Smith[9], the circulation across the wake segment a-b-c-d remains constant :

$$\Gamma = \oint_{\Omega} U \mathrm{d}s = \mathrm{ab}\Delta U = \mathrm{constant}$$

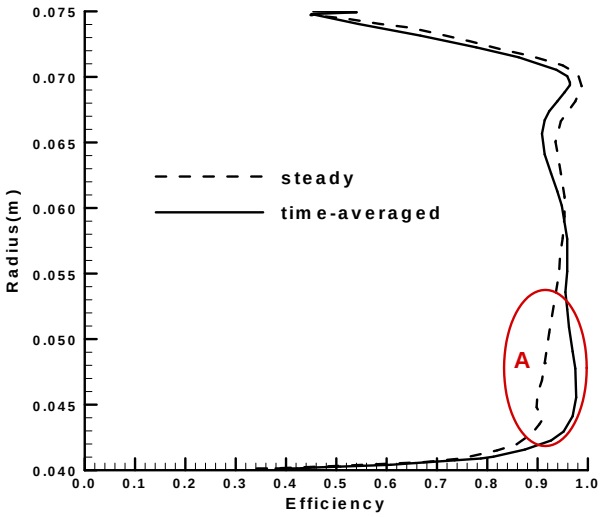

Figure. 8 Distribution of Isentropic Efficiency along Blade Span

Under the assumption of incompressible and inviscid flow, to have the constant circulation, the velocity defect in the wake has to change inverse proportion to the wakes length. As the wake segment passes through the downstream passage, it would be tilted and stretched because of the difference in velocity between suction and pressure side and the diffusive shape of vane. So the wake length grows longer, which results in smaller velocity defect and less flow loss. This is called wake recovery. Though the velocity difference between suction and pressure surface is small for the test case in this paper, this phenomenon can also be found in Fig. 5 by careful observation. For further study of the influences of the unsteady disturbance on the efficiency, the comparison of isentropic efficiency along the blade span between time-averaged HB solution and steady solution is illustrated in Fig. 8.

It could be found that the isentropic efficiency obtained by HB below mid-span is higher than that from steady calculation, while a contrary relationship exists above mid-span. To explain this interesting phenomenon, a parameter *k* which could be used to describe the intensity of unsteady disturbance is introduced here:

$$k = \sqrt{u'^2 + v'^2 + w'^2} / U_{tip}$$

Where, u'、v'、w' are the fluctuating velocity in three directions respectively, U_{tip} is the blade tip speed (103m/s in this work). The instantaneous contour of *k* at row2 inlet is showed in Fig. 9.

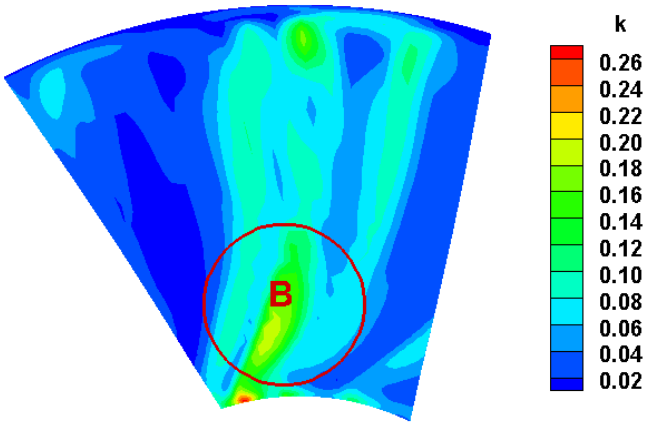

Figure. 9 Contour of k at Row2 Inlet

The wake from row 1 can be identified clearly in Fig.9, and it shows that the disturbance caused by the upstream wake is the dominant part of unsteady perturbation. Meanwhile, Fig.9 also indicates that the intensity of wake disturbance weakens along blade span. Combining Fig.8 and Fig.9, it can be found that a higher value of *k* is corresponding to higher efficiency below mid-span, i.e., the circle region B in Fig.9 agrees with the ellipse region A in Fig.8. However, this law is invalid above mid-span.

For most of transonic compressors/fans, the work is done by changing the velocity direction near blade root and by shock compression near blade tip. So the difference of velocity between suction and pressure side is bigger at the position near blade root. It results that the upstream wake near the stall is tilted and stretched more than that near the blade tip. Consequently, the wake recovery near blade root is stronger and the isentropic efficiency is higher.

As for the low efficiency near blade tip comprising the steady one, it should be attributed to a couple of reasons. The first reason is explained as above, i.e. the feeble wake recovery. The second reason is that the upstream wake interacts with the boundary and the downstream wake.

Fig. 10 shows the entropy contours at three moments. Firstly, taking a look at the contours at 85% span, it is clear that, at time A, the entropy flow caused by upstream wake is in blade passage, and it thickens the boundary layer on the suction surface and leads to efficiency loss (entropy production). At time B, the wake entropy flow passes through the row 2 wake and enlarges the area of high entropy value. At time C, the wake entropy continues to spread and interact with the row2 wake. It is obviously that the process of interaction between row 1 wake and row 2 wake increases entropy a lot and leads to serious efficiency loss at 85% blade span. Then turning attention to the contours at 15% span, though there is a similar phenomenon in Fig.10, the entropy increased by the wake interaction is tiny and the resulting efficiency loss is exceeded by efficiency gains due to the strong wake recovery. Above all, the wake recovery is dominant below mid-span, while the wake interaction is dominant above mid-span.

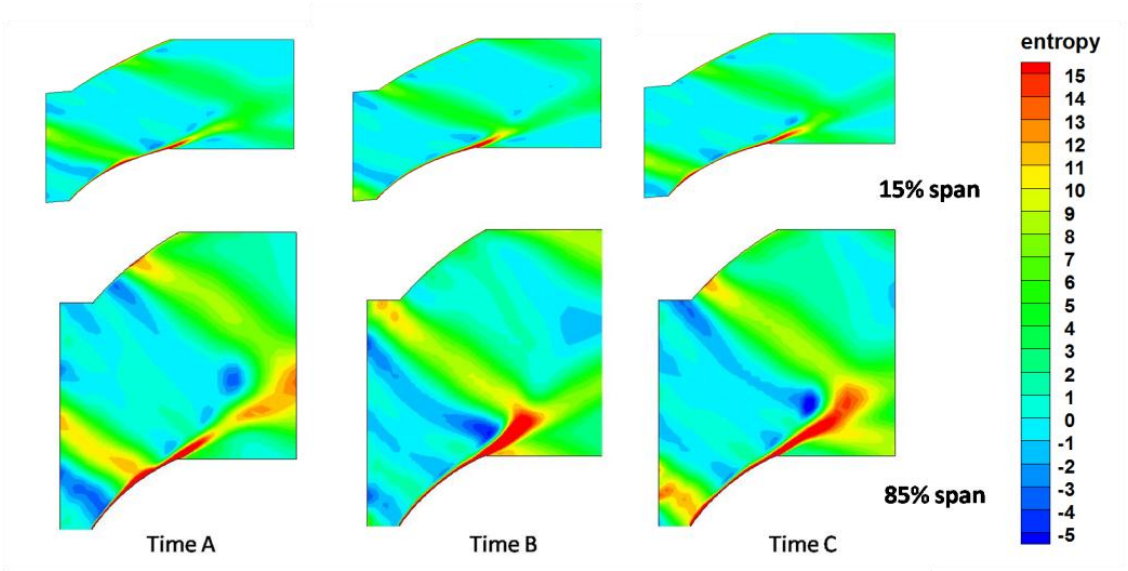

Figure. 10 Entropy of Three Moments at 15% and 85% Blade Span

V. CONCLUSION

This paper applies harmonic balance method to simulate the original-designed two stage counter-rotating fan. The unsteady characteristic, row interaction and wake spread have been studied, the discussions show that: the upstream wake improves the efficiency of row 2 below the mid-span because of the wake recovery, while it lowers the efficiency above the mid-span because of interaction between row1 and row 2 wake; It is meaningful to study how to make use of the unsteady effects; The harmonic balance method is efficient and reliable to simulate the periodic unsteady blade row interaction.

REFERENCES

[1] Adamczy, J. J., Model Equations for Simulating Flows in Multistage Turbomachinery. *ASME Paper, 85-GT-226*, 1985
[2] Hall, K., Lorence, C., Calculation of Three-dimensional Unsteady Flows In Turbomachinery Using the Linearized Harmonic Euler equations. *Journal of Turbomachinery, 115(4)*, 1993, 800-809
[3] Hall, K., Thomas, J., Clark, W., Computation of Unsteady Nonlinear Flows in Casecades using a Harmonic Balance Technique. *AIAA Journal, 40(5)*, 2002, 879-886
[4] McMullen, M., Jameson, A., Alonso, J., Demonstration of Nonlinear Frequency Domain Methods. *AIAA Journal, 40(7)*, 2006, 1428-1435
[5] He, L., Harmonic Solution of Unsteady Flow around Blade with Separation. *AIAA Journal, 46(6)*, 2008, 1299-1307
[6] Giles, M. B., Nonreflecting Boundary Conditions for Euler Equation Calculations, *AIAA Journal*, 28(12), 1990, 2050-2058
[7] Erdos, J.I., Alznert, E., McNally, W., Numerical Solution of Periodic Transonic Flow through a Fan Stage, *AIAA Journal, 15(11)*, 1977, 1559-1568
[8] Tyler, J., Sofrin, T., Axial Flow Compressor Noise Studies. *Society of Automotive Engineers Transactions, 70*, 1962, 307-332
[9] Smith, L.H., Wake Dissipation in Turbomachines, *Journal of Basic Engineering, Vol. 88D*, 1966, 688-690